

Article

Facile Fabrication of Bio-Nanohybrid Electrode with Guanine/Cytosine-Modified Electrochemically Reduced Graphene Oxide Electrode and Its Application in Doxorubicin Analysis

Yoojin Cho ^{1,†}, Da Eun Oh ^{1,†} , Myungeun Kim ², Ahran Lim ², Chang-Seuk Lee ^{2,*}  and Tae Hyun Kim ^{1,*} ¹ Department of Chemistry, Soonchunhyang University, Asan 31538, Republic of Korea² Department of Chemistry, Seoul Women's University, Seoul 01797, Republic of Korea

* Correspondence: cslee.chem@swu.ac.kr (C.-S.L.); thkim@sch.ac.kr (T.H.K.);

Tel.: +82-2-970-5655 (C.-S.L.); +82-41-5304722 (T.H.K.)

† These authors contributed equally to this work.

Abstract: Graphene, known for its outstanding physical and chemical properties, is widely used in various fields, including electronics and biomedicine. Reduced graphene oxide (rGO) is preferred for electrochemical applications due to its enhanced water solubility and dispersion. Electrochemically reduced graphene oxide (ErGO) is particularly advantageous as it can be prepared under mild conditions and simplifies sensor fabrication; however, ErGO-based electrochemical sensors often lack specificity. Bioreceptors like proteins, enzymes, and DNA/RNA aptamers are incorporated to provide high specificity. This study introduces a guanine (G)/cytosine (C)-modified ErGO electrode (G/C@ErGO-GCE) for the sensitive electrochemical detection of doxorubicin (DOX) with good selectivity. The G/C mixture acts as a bioreceptor and is anchored on the ErGO-GCE surface via π - π interactions. The G/C@ErGO-GCE was characterized using scanning electron microscopy, contact angle measurement, Raman spectroscopy, and electrochemical methods. The sensor demonstrated excellent dynamic range (DPV: 10 nM to 1 μ M, CA: 30 nM to 1.3 μ M), sensitivity (DPV: 2.17 μ A/ μ M, CA: 6.79 μ A/ μ M), limit of detection (DPV: 84 nM, CA: 34 nM), and selectivity for DOX detection, highlighting its potential for biomedical applications and pharmacokinetic studies.



Citation: Cho, Y.; Oh, D.E.; Kim, M.; Lim, A.; Lee, C.-S.; Kim, T.H. Facile Fabrication of Bio-Nanohybrid Electrode with Guanine/Cytosine-Modified Electrochemically Reduced Graphene Oxide Electrode and Its Application in Doxorubicin Analysis.

Chemosensors **2024**, *12*, 163.<https://doi.org/10.3390/chemosensors12080163>

chemosensors12080163

Received: 7 July 2024

Revised: 14 August 2024

Accepted: 15 August 2024

Published: 16 August 2024



Copyright: © 2024 by the authors. Licensee MDPI, Basel, Switzerland. This article is an open access article distributed under the terms and conditions of the Creative Commons Attribution (CC BY) license (<https://creativecommons.org/licenses/by/4.0/>).

Keywords: bio-nanohybrid electrode; reduced graphene oxide; single nucleotides; doxorubicin; anticancer drug

1. Introduction

Graphene is a powerful nanomaterial with wide applications ranging from electronics to biomedical fields [1–4]. It offers several advantages, including excellent thermal/electrical conductivity, mechanical strength, flexibility, a large surface-area-to-volume ratio, and chemical stability [5,6]. Graphene is often modified with various atoms, such as oxygen, nitrogen, and sulfur, depending on the intended application; doping with these atoms alters its optical, mechanical, and electronic properties [7–10]. In electrochemical applications, graphene is typically used in the form of reduced graphene oxide (rGO) due to its good solubility in water, good dispersion, and numerous oxide functional groups. Several methods exist for preparing rGO, including hydrothermal reduction, chemical reduction, and electrochemical reduction [11–14]. Hydrothermal and chemical reductions require harsh conditions, such as high temperatures and toxic reducing agents, while electrochemically reduced graphene oxide (ErGO) is prepared under milder conditions with a neutral pH of 7.0 and a simple supporting electrolyte [13–15]. Furthermore, during the preparation of ErGO, GO is deposited onto electrode surfaces, which can simplify the sensor fabrication process by eliminating the rGO transfer step. However, the practical application of ErGO-based biosensors is limited by their lack of specificity in electrochemical reactions.

To address this lack of specificity, modifications with recognition elements, including chelating ligands, proteins, and DNA/RNA, are introduced to ErGO-based electrochemical sensors. Recognition elements for biomaterials (bioreceptors), including proteins, enzymes, peptides, and DNA/RNA aptamers, provide superior specificity for target biomaterials in complex biofluids [16–19]. Purine- and pyrimidine-based single nucleotides have π -electrons and functional groups of amine and oxygen, which can selectively bind certain chemicals via π - π interactions and hydrogen bonding [20–22]. Furthermore, single nucleotides are chemically and structurally stable under physiological conditions, allowing for selective binding to target molecules when immobilized onto sensing platforms. Specifically, the guanine (G) and cytosine (C) pair is known to bind selectively with doxorubicin (DOX) due to DOX's ability to intercalate with the G-C pairs [23]. The specificity of DOX for the G-C base pair in DNA can be determined by various structural and chemical factors (Scheme S1). These include hydrogen bonding and base pairing stability, π - π stacking interaction, electrostatic and Van der Waals interactions, sequence preference, and thermodynamic considerations [24–26]. More specifically, G-C pairs in DNA are connected by three hydrogen bonds, making them more thermodynamically stable and rigid than adenine–thymine (A-T) pairs. The amino group on guanine can interact with the carbonyl and hydroxyl groups on the sugar moiety of doxorubicin, enhancing binding specificity. DOX possesses a planar aromatic structure that enables π - π stacking interactions with the planar aromatic bases in DNA. These interactions are stronger with G-C pairs due to their greater electronic density compared to A-T pairs. Additionally, DOX carries a positive charge on its amino sugar moiety, which can form electrostatic interactions with the negatively charged phosphate backbone of DNA. G/C-rich regions tend to have a more compact structure, bringing the phosphate backbones closer together, which can enhance electrostatic interactions. Furthermore, the close contact between the flat surfaces of doxorubicin and the base pairs allows for Van der Waals forces to play a significant role in binding specificity. These interactions are more favorable in the presence of the more stable G-C pairs. Therefore, incorporating the bioreceptor G/C with the nanomaterial ErGO to form a bio-nanohybrid composite (G/C@ErGO) results in superior performance in both biorecognition and electrochemical activity.

DOX is a widely used chemical drug for cancer chemotherapy that needs to be monitored in biological fluids for pharmacokinetic studies [27]. DOX possesses useful chemical characteristics for convenient detection with analytical instruments, such as intrinsic fluorescence, a red color, numerous oxygen functional groups, free π -electrons, and electrochemical activity. Several analytical methods for DOX monitoring have been investigated, including fluorescence spectroscopy, chromatography, mass spectrometry, and electrochemical detection [28–31]. Electrochemical detection of DOX offers numerous advantages, including small-sized instrumentation, simple operation procedures, a fast response, and less invasive sampling, whereas other analytical methods require large instruments, complex sample preparation, and long detection times.

In our previous report, we fabricated low-defect graphene (LDG) using shear exfoliation and demonstrated the electrochemical sensing performance of an LDG electrode for detecting DOX [28]. The shear exfoliation method is suitable for the mass production of graphene with low defects; however, it is limited by complicated pre-treatment procedures (e.g., removing organic solvents and redispersion in aqueous media). Furthermore, the sensing mechanism for DOX relies solely on π - π interactions, indicating a lack of interaction between the working electrode and the target analyte. Consequently, the LDG electrode showed limited sensing performance in terms of sensitivity, linear range, and limit of detection. Therefore, while the previous result is more appropriate for the industrial-scale synthesis of graphene, it is less suitable for electroanalytical chemistry.

Here, we demonstrate the use of a G/C-modified ErGO electrode for the selective and sensitive electrochemical detection of DOX. A single-nucleotide G/C mixture is modified onto the ErGO-glassy carbon electrode (GCE) surface through π - π interaction, forming a bio-nanohybrid electrode (G/C@ErGO-GCE) (Scheme 1). The fabricated G/C@ErGO-GCE

was characterized for its physical and electrochemical properties using various analytical methods, such as contact angle measurement, scanning electron microscopy, atomic force microscopy, Raman spectroscopy, X-ray photoelectron spectroscopy, IR spectroscopy, cyclic voltammetry, and electrochemical impedance spectroscopy. We further propose an electrochemical sensing mechanism for DOX, utilizing a G/C-modified ErGO bio-nanohybrid composite as a selective recognition element and electrocatalytic material. Briefly, the single nucleotide mixture of G/C can attract DOX via various interactions, such as hydrogen bonding, base pairing stability, π - π stacking interactions, electrostatic and Van der Waals interactions, sequence preference, and thermodynamic considerations, thereby increasing the mass transport of DOX [24–26,32–34]. The ErGO electrode then acts as an electrocatalyst, enhancing electron transfer to DOX. These effects, facilitated by the G/C@ErGO bio-nanohybrid, make the sensor both sensitive and selective. This G/C@ErGO-GCE sensor demonstrated excellent sensitivity and selectivity for the electrochemical determination of DOX, indicating that this biosensor has exceptional potential for biomedical applications and pharmacokinetic studies.



Scheme 1. Schematic diagrams for the facile fabrication of bio-nanohybrid composite of G/C@ErGO-GCE electrode.

2. Materials and Methods

2.1. Materials

Graphite powder, potassium permanganate (KMnO_4), NaNO_3 , KCl , NaCl , CaCl_2 , potassium ferricyanide(III) ($\text{K}_3\text{Fe}(\text{CN})_6$), hexaammineruthenium(III) chloride ($\text{Ru}(\text{NH}_3)_6\text{Cl}_3$), urea, glucose, guanine, cytosine, phosphate-buffered saline (PBS) powder, and doxorubicin were sourced from Sigma-Aldrich Co. (St. Louis, MO, USA). Other chemicals, including sodium hydroxide (NaOH), hydrogen peroxide (H_2O_2), and sulfuric acid (H_2SO_4) were acquired from Duksan Pure Chemicals Co. (Ansan, Gyeonggi-do, Republic of Korea). All reagents were of analytical grade and used as received without additional purification. Deionized (DI) water was utilized for all experiments.

2.2. Instruments

Electrochemical measurements were conducted using a CHI 660D electrochemical workstation (CH Instruments, Inc., Austin, TX, USA, Z-202306208148) at the Research Support Center for Bio-Bigdata Analysis and Utilization of Biological Resources. The surface characteristics of the fabricated electrodes were examined with a scanning electron microscope (SEM, JEOL JSM 5600 LV, Tokyo, Japan), X-ray photoelectron spectroscopy (XPS, ESCA 2000, Thermo VG Scientific, Cheshire, UK), and atomic force microscopy (AFM, Park Systems Corp., NX10, Suwon, Republic of Korea, 202308038870) at the Research Support Center for Bio-Bigdata Analysis and Utilization of Biological Resources. Raman spectroscopy was carried out using an EnSpectr R532 Raman spectrometer (Enhanced Spectrometry, Inc., Meridian, ID, USA). Contact angle measurements were performed with a contact angle analyzer (Phoenix Mini, SEO Co., Ltd., Suwon, Republic of Korea).

2.3. Electrochemical Measurements

A traditional three-electrode setup was employed at ambient temperature, consisting of a Pt wire as the counter electrode, a Ag/AgCl electrode as the reference electrode, and glassy carbon electrode (GCE), ErGO-GCE, and G/C@ErGO-GCE as the working electrodes. First, the ErGO-modified GCE was fabricated using cyclic voltammetry (CV), sweeping a negative potential from -1.5 to 0.0 V (vs. Ag/AgCl) in a 0.1 M KNO_3 solution containing 0.3 mg/mL GO.

For the electrochemical characterization, CV measurements were sweeping a potential from -0.2 to 0.6 V (vs. Ag/AgCl) with a scan rate of 0.01 V/s in a 0.1 M KNO_3 supporting electrolyte containing 5 mM $\text{Fe}(\text{CN})_6^{3-}$ and 5 mM $\text{Ru}(\text{NH}_3)_6^{3+}$. Electrochemical impedance spectroscopy (EIS) measurements were performed at the initial potential, calculated as $((E_{pc} + E_{pa})/2)$ from CV, under the following conditions: frequency range from $10,000$ to 1 Hz and an amplitude of 0.005 V.

For the electrochemical detection of DOX, differential pulse voltammetry (DPV) measurements were conducted in the potential range from -0.1 to 0.8 V (vs. Ag/AgCl) with the following settings: pulse amplitude of 60 mV, potential increment of 7 mV, pulse width of 50 ms, sample width of 0.5 ms, and pulse period of 0.5 s. Then, chronoamperometry (CA) measurements were performed at a potential of 0.35 V (vs. Ag/AgCl) with sample intervals of 0.1 s and a quiet time of 20 s.

2.4. Preparation of G/C@ErGO-GCE Bio-Nanohybrid Electrode

Graphene oxide (GO) was prepared using graphite powders by the modified Hummers method [35,36]. Briefly, a $2:1$ (w/w) ratio of graphite flakes to NaNO_3 was pre-mixed. The graphite- NaNO_3 mixture was added to a beaker containing a predetermined amount of H_2SO_4 (99.9 wt.%) maintained at room temperature. The mixture was stirred continuously for 1 h to form a homogeneous suspension. The excess KMnO_4 was slowly added to at least 3 times the amount of graphite- NaNO_3 mixture at 40 °C for 12 h with stirring. After that, the mixture was diluted with 50 mL of DI water, and 28% H_2O_2 aqueous solution was added to close the reaction. After closing the reaction, the GO solution was purified via centrifugation for several times at $13,500$ rpm. Finally, the purified GO dispersion was diluted to a final concentration of 1.0 mg/mL using DI water. To achieve a homogeneous exfoliation, the 1.0 mg/mL GO dispersion in DI water was sonicated for 1 h, resulting in a yellowish-brown colored solution.

GCE was sequentially polished with alumina powder of 1.0 , 0.3 , and 0.05 μm particle size to achieve a mirror-like finish. It was then sonicated for 1 min in a $1:1$ (v/v) ethanol and DI water mixture. Following the polishing steps, the GCE was electrochemically pre-treated in 0.25 M H_2SO_4 solution using cyclic voltammetry (CV). The CV involved potential cycling from -1.0 to 1.0 V (vs. Ag/AgCl) at 50 mV/s for 20 cycles to clean the electrode surface. The electrochemical deposition ErGO on the clean GCE was performed in 10 mM of PBS containing 0.3 mg/mL of GO with CV from -1.5 to 0.0 V (vs. Ag/AgCl) at 10 mV/s for 3 cycles (Figure 1A). To remove any weakly adsorbed GO and improve the attachment of ErGO onto the GCE surface, the ErGO-GCE was thoroughly rinsed with DI water to remove residual salts. Subsequently, it was dried under an infrared (IR) lamp to promote solvent evaporation and potentially strengthen the interaction between ErGO and the GCE surface.

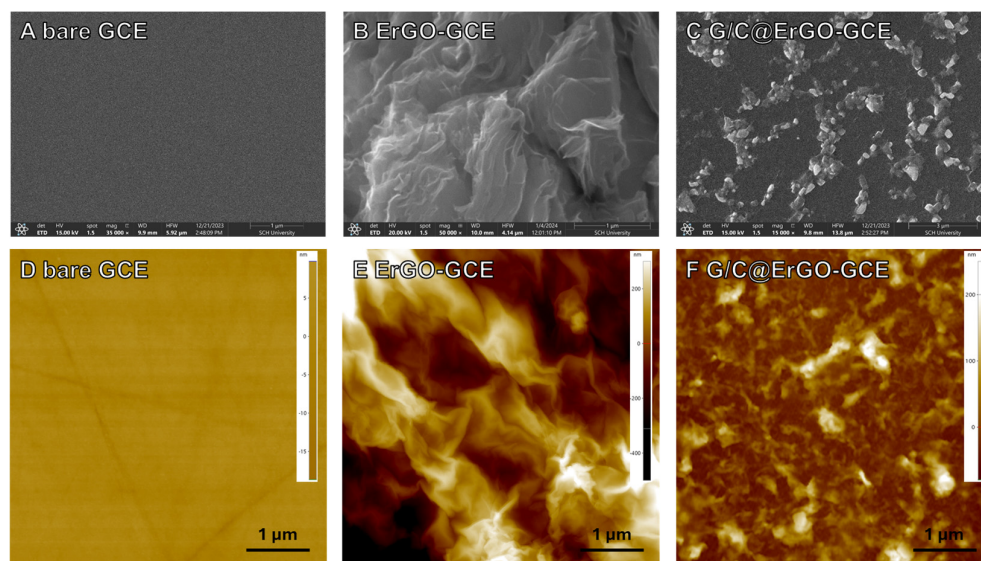


Figure 1. SEM images of (A) bare GCE, (B) ErGO-GCE, and (C) G/C@ErGO-GCE. AFM images of (D) bare GCE, (E) ErGO-GCE, and (F) G/C@ErGO-GCE.

3. Results and Discussion

3.1. Preparation and Characterization

First, the ErGO-modified GCE was fabricated using CV, sweeping a negative potential from -1.5 to 0.0 V (vs. Ag/AgCl) in a 0.1 M KNO_3 solution containing 0.3 mg/mL GO. Figure S1 shows the cyclic voltammograms; the reduction peaks near -1.2 V decrease with the number of cycles, representing the number of oxygen groups on graphene decreasing. Through this experiment, we confirm that the ErGO-GCE working electrode is ready for the next functionalization step.

Subsequently, single nucleotides of guanine (G) and cytosine (C) were immobilized onto the ErGO-GCE by the drop-casting method. A Tris-HCl buffered solution containing G and C at a specific ratio was prepared for the ErGO-GCE surface functionalization. Single nucleotides, G and C, immobilized onto the ErGO surface via π - π stacking form the bio-nano hybrid composite with ErGO. To confirm the morphology of the ErGO-GCE decorated with single nucleotides G and C, SEM was employed (Figure 1A–C). The SEM image of ErGO-GCE shows a well-dispersed wrinkled structure with bright edges, indicating both successful fabrication of ErGO-GCE and good electron transport characteristics (Figure 1B). Figure 1C depicts the surface morphology of G/C@ErGO-GCE, showing a smoother surface compared to ErGO-GCE, with bright particles of G and C, well-dispersed onto the electrode surface, indicating the successful immobilization of single nucleotides and good electron transfer characteristics [37].

The surface morphology of the electrodes was further characterized using atomic force microscopy (AFM). Figure 1D–F shows the AFM images of bare GCE, ErGO-GCE, and G/C@ErGO-GCE. The AFM image of ErGO-GCE shows a rough surface morphology with high differences in depth (Figure 1E), while bare GCE shows a flatter surface (Figure 1D). Figure 1F shows the AFM image of G/C@ErGO-GCE with a smoother surface morphology compared to ErGO-GCE, indicating the successful immobilization of single nucleotides G and C. For the quantitative analysis of height differences among these electrodes, we compare the deviations in height differences obtained from AFM measurements. Figure S2 shows the comparison of height differences among the working electrodes of bare GCE, ErGO-GCE, and G/C@ErGO-GCE. The height differences in each electrode were examined as 5.11 nm, 508.07 nm, and 169.41 nm for bare GCE, ErGO-GCE, and G/C@ErGO-GCE, respectively. The height difference in ErGO-GCE increased after functionalization with ErGO due to the rough surface morphology nature of ErGO. After immobilization of G and C, the height difference decreased. This is because the single nucleotides G and C cover

the ErGO-GCE surface by forming a bio-nanohybrid composite. From these results, we confirm that our fabrication process was well-designed to produce G/C@ErGO-GCE.

The electrode was designed for use in an aqueous supporting electrolyte; therefore, wettability is an important factor in determining sensing performance. The wettability of the electrode surface was assessed through contact angle measurement. The contact angle of ErGO-GCE was measured at 80° , while bare GCE showed a contact angle of 71° (Figure 2A). These contact angle measurements indicate the successful removal of oxygen groups from GO. The G/C@ErGO-GCE showed a decreased contact angle of 66° compared to ErGO-GCE, resulting in increased wettability due to the surface being decorated with G and C. This result indicates that the fabricated G/C@ErGO-GCE is suitable for use as an electrochemical biosensor operating in an aqueous system.

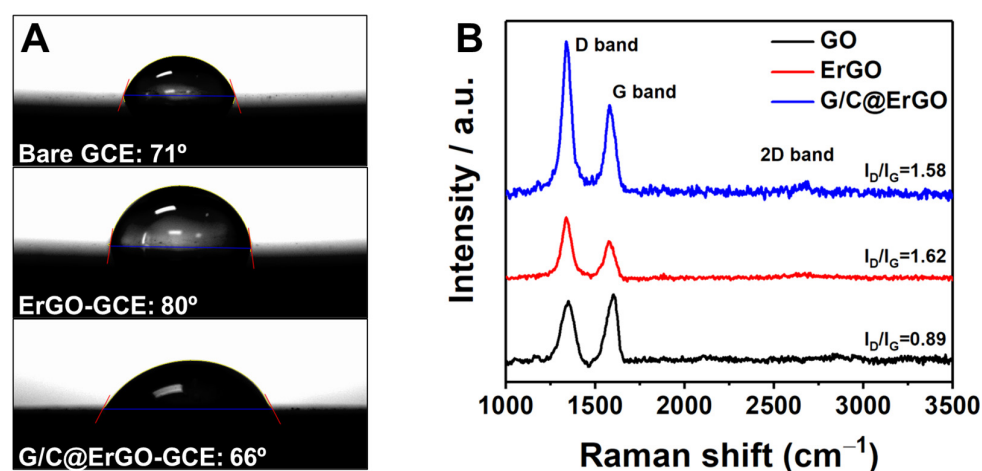


Figure 2. (A) Contact angle measurement. (B) Raman spectra of GO, ErGO, and G/C@ErGO.

Raman spectroscopy was introduced to verify the quality of the bio-nanohybrid composite of G/C@ErGO. Raman spectrum of GO exhibited a well-defined D band at 1350 cm^{-1} and G band at 1602 cm^{-1} (Figure 2B). These two bands are key factors in determining the physical and chemical characteristics of graphene; the D band correlates with defects derived from grain boundaries, vacancies, and amorphous carbon, while the G band is assigned to an E_{2g} mode of graphite. These characteristic bands were distinctly shown in Raman spectra of ErGO (D band: 1337 cm^{-1} , G band: 1575 cm^{-1}) and G/C@ErGO (D band: 1337 cm^{-1} , G band: 1580 cm^{-1}) [38,39]. Furthermore, the intensity ratio of the D and G bands (I_D/I_G) indicates the number of defects in sp^2 carbon atoms. The I_D/I_G value of ErGO increased from 0.89 to 1.62 after the electrochemical reduction of GO, implying a decreased number of oxygen groups and an increased number of smaller graphene domains in ErGO. Following the immobilization of G and C, there were negligible changes in the I_D/I_G value, indicating that the adsorption of G and C does not compromise the quality of ErGO [40]. These results suggest that the fabricated G/C@ErGO bio-nanohybrid composite has suitable characteristics for an electrode material.

The chemical characterization was performed using X-ray photoelectron spectroscopy (XPS) for detailed elemental analysis during the fabrication of the G/C@ErGO bio-nanohybrid composite. Figure 3A shows the survey scans of ErGO and G/C@ErGO, revealing the presence of C, O, and N. Specifically, the high-resolution spectra of C1s for ErGO and G/C@ErGO show four typical peaks: C=C (284.4 eV), C-O (285.3 eV), O-C=O (288.0 eV), and C=O (290.0 eV) (Figure 3B,C). Among these peaks, C=C, C-O, and O-C=O peaks are present in both spectra of ErGO and G/C@ErGO, while the C=O peak appears only in G/C@ErGO. The C=O bond from G and C increases the intensity in the XPS analysis. The N1s peak appears in the survey scan of G/C@ErGO due to the nitrogen atoms in G and C. Furthermore, the deconvoluted N1s spectrum shows two peaks: -NH (398.9 eV) and -NH₂

(400.2 eV). These results indicate that G and C are successfully immobilized onto ErGO surfaces, forming the bio-nano hybrid composite.

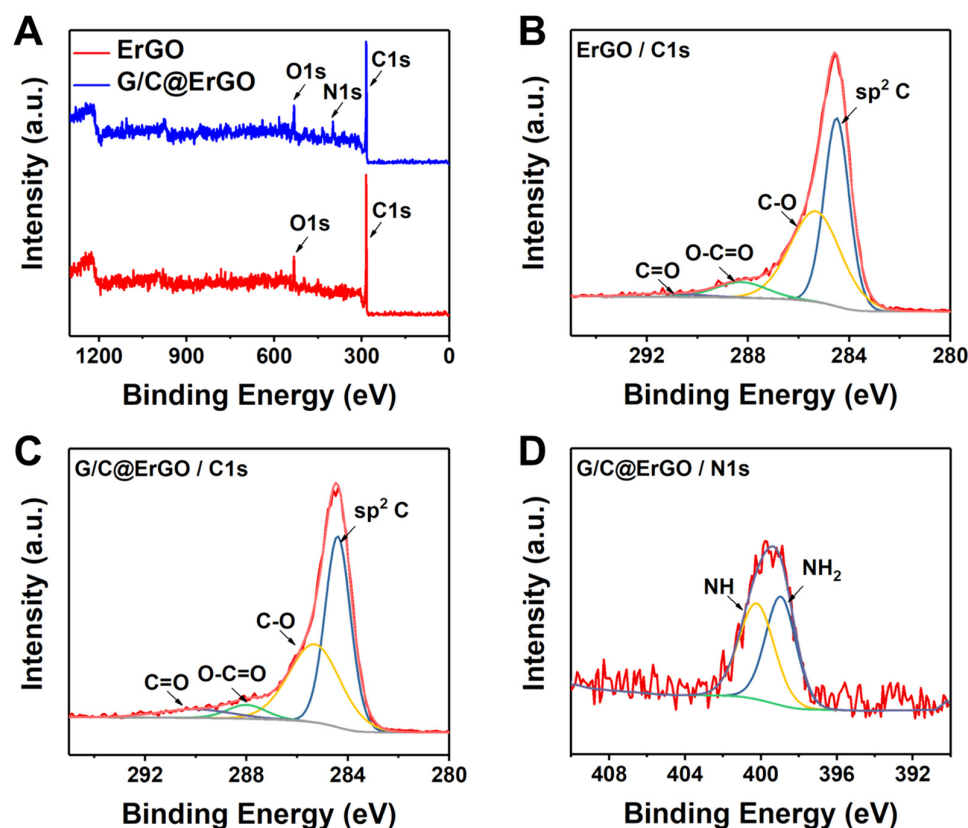


Figure 3. XPS analysis of (A) survey scans for ErGO and G/C@ErGO, (B) C1s from ErGO, (C) C1s from G/C@ErGO, and (D) N1s from G/C@ErGO.

3.2. Electrochemical Property of G/C@ErGO-GCE

The electrode surface modification with nanomaterials, charged chemicals, and receptor molecules gives specific interaction to the target molecules. The electrochemical characterization of G/C@ErGO-GCE was performed using CV and electrochemical impedance spectroscopy (EIS). Figure 4A,C shows cyclic voltammograms obtained from 5 mM $\text{Fe}(\text{CN})_6^{3-}$ and 5 mM $\text{Ru}(\text{NH}_3)_6^{3+}$ with bare GCE, ErGO-GCE, and G/C@ErGO-GCE, respectively. The redox peak current of $\text{Fe}(\text{CN})_6^{3-}$ and $\text{Ru}(\text{NH}_3)_6^{3+}$ increased after functionalized ErGO due to the large surface area and electrochemical catalytic character of ErGO. Typically, the adsorption of biomaterials onto the electrode reduces the active sites of the electrode. However, the resulting cyclic voltammograms showed negligible changes in peak current, indicating minor changes in the electrochemical active sites of the electrode.

The purine and pyrimidine bases serve as binding linkers for the immobilization of G and C onto the ErGO surface via π - π interactions. To confirm the successful immobilization of G and C, we introduced electrochemical impedance spectroscopy (EIS). EIS provides information such as solution resistance, charge transfer resistance (R_{ct}), electrode surface charges, capacitance, and Warburg impedance. Here, we used EIS to confirm the successful immobilization of G and C by comparing R_{ct} among bare GCE, ErGO-GCE, and G/C@ErGO-GCE working electrodes. Figure 4B,D shows the Nyquist plots obtained from EIS, performed using the electrochemically active species and the working electrode. The R_{ct} was examined at each step of G/C@ErGO-GCE fabrication with two different electrochemically active species, $\text{Fe}(\text{CN})_6^{3-}$ and $\text{Ru}(\text{NH}_3)_6^{3+}$. The R_{ct} between the working electrodes and $\text{Fe}(\text{CN})_6^{3-}$ significantly increased to 794.7 Ω for G/C@ErGO-GCE, while bare GCE and ErGO-GCE showed smaller R_{ct} values of 103.0 Ω and 128.4 Ω , respectively. On the other hand, the R_{ct} between the working electrodes and $\text{Ru}(\text{NH}_3)_6^{3+}$ gradually

decreased from 1222 Ω and 1363 Ω to 868.1 Ω when using bare GCE, ErGO-GCE, and G/C@ErGO-GCE, respectively. These changes in surface charge were caused by the charged single nucleotides G and C, which also provide a specific interaction with DOX. These results confirm the successful fabrication of G/C@ErGO-GCE and its suitability for the electrochemical detection of DOX.

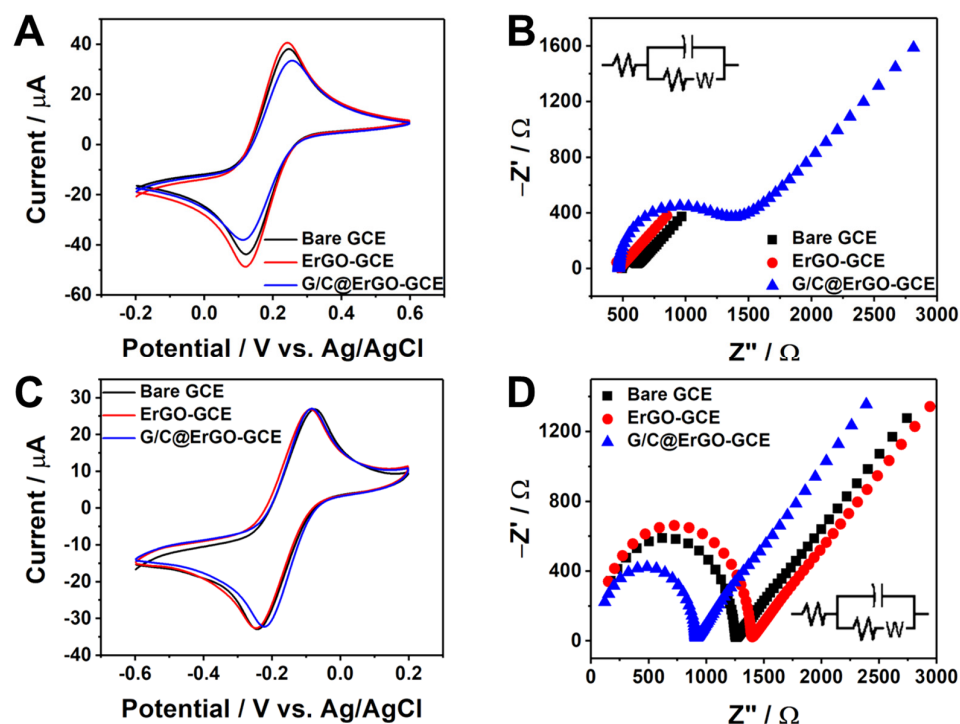


Figure 4. (A) Electrochemical characterization of bare GCE, ErGO-GCE, and G/C@ErGO-GCE with 0.1 M KNO₃ supporting electrolyte containing 5 mM Fe(CN)₆³⁻ and (C) 5 mM Ru(NH₃)₆³⁺. Nyquist plots obtained from EIS for each working electrode of bare GCE, ErGO-GCE, and G/C@ErGO-GCE with 0.1 M KNO₃ supporting electrolyte containing (B) Fe(CN)₆³⁻ and (D) Ru(NH₃)₆³⁺. Inset: a Randles equivalent circuit diagram.

3.3. Electrochemical Detection of DOX

Prior to using G/C@ErGO-GCE, the G/C content ratio must be optimized. To achieve this, differential pulse voltammetry (DPV) response over DOX was utilized. The G/C content ratios tested were 10:0, 1:9, 3:7, 5:5, 7:3, 9:1, and 0:10. As shown in Figure S3, seven different calibration curves for DOX detection using DPV were generated. The sensitivity (slope), standard deviation, and R² value for DOX detection were key parameters for optimizing the G/C content ratio. The 1:9 G/C content ratio was selected as the optimal value due to its high sensitivity of 0.23 μ A/nM, low standard deviation, and high R² value of 0.996 among the tested ratios.

For the determination of DOX, electrochemical methods of differential pulse voltammetry (DPV) and chronoamperometry (CA) were introduced. Figure 5A shows the DPV response of the G/C@ErGO-GCE in 0.1 M KNO₃ with successive additions of different concentrations of DOX, ranging from 10 nM to 1 μ M. The corresponding calibration curve was obtained as a function of DOX concentration using the anodic peak current (Figure 5B). The oxidation peak current increased with the increasing concentration of DOX. The sensing performance of G/C@ErGO-GCE for DOX detection was determined to have a sensitivity of 2.17 μ A/ μ M, linear range of 0.01 to 1.0 μ M, and a limit of detection (LOD) of 84.4 nM. The G/C@ErGO-GCE demonstrated superior sensing performance compared to the bare GCE and ErGO-GCE (Figure S4). Figure 5C depicts the typical amperometric response of G/C@ErGO-GCE upon the addition of DOX at a selected potential of 0.35 V. The biosensor showed a rapid current response, achieving a dynamic equilibrium of the current signal

within 5 s after DOX addition, reflecting fast electron transfer between G/C@ErGO-GCE and DOX. The corresponding calibration curve was obtained as a function of DOX concentration using the current response of DOX. The sensing performance of G/C@ErGO-GCE for DOX detection was determined to have a sensitivity of $6.79 \mu\text{A}/\mu\text{M}$, linear range of 0.03 to $1.3 \mu\text{M}$, and a LOD of 34.9 nM . Table 1 shows a comparison of the DOX detection performance of G/C@ErGO-GCE with that of other existing biosensors.

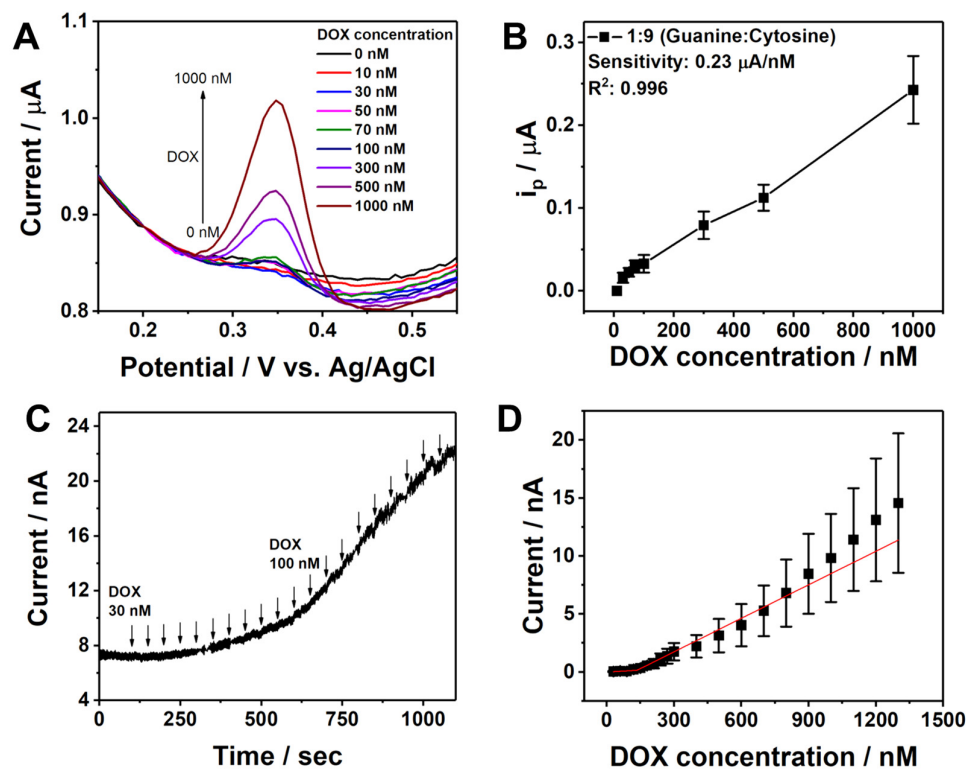


Figure 5. Electrochemical detection of DOX with G/C@ErGO-GCE using (A) DPV and (C) chronoamperometry. (B,D) Corresponding calibration curves for the electrochemical detection of DOX with DPV and chronoamperometry, respectively.

Table 1. Comparison of various electrode materials for the electrochemical detection of DOX.

Electrode Materials	Method	Linear Range (μM)	Sensitivity ($\mu\text{A}/\mu\text{M}$)	Limit of Detection (μM)	Ref.
Carbon dots/magnesium oxide	¹ CV	0.1~1.0	-	0.09	[41]
AgNP/poly(chitosan)	² SWV	0.103~5.17	0.8028	0.103	[42]
UiO-66-NH ₂ /MWCNTs	³ DPV	0.1~75	0.01829	0.051	[43]
rGO/AuNPs	SWV	0.3~6.0	0.385	0.1	[44]
p-AgSAE	DPV	1.0~40	0.024	0.84	[45]
LDG	DPV	0.3~2.7	0.723	0.039	[31]
	⁴ CA	0.3~2.7	-	0.653	
G/C@ErGO	DPV	0.01~1.0	2.17	0.084 (DPV)	Present work
	CA	0.03~1.3	6.79	0.034 (CA)	

¹ CV: cyclic voltammetry; ² SWV: square wave voltammetry; ³ DPV: differential pulse voltammetry; ⁴ CA: chronoamperometry.

3.4. Analytical Performance

To examine the analytical performance of G/C@ErGO-GCE, several tests were conducted, including reproducibility, selectivity, stability, and real-sample detection. Reproducibility represents the reliability and precision of the sensor fabrication procedures and is evaluated by comparing electrochemical signals from different sensors. Figure 6A depicts

the result of reproducibility with five different sensors, showing a reasonable average relative standard deviation (RSD) of 7.53%, indicating that our sensor fabrication procedures are reliable and precise.

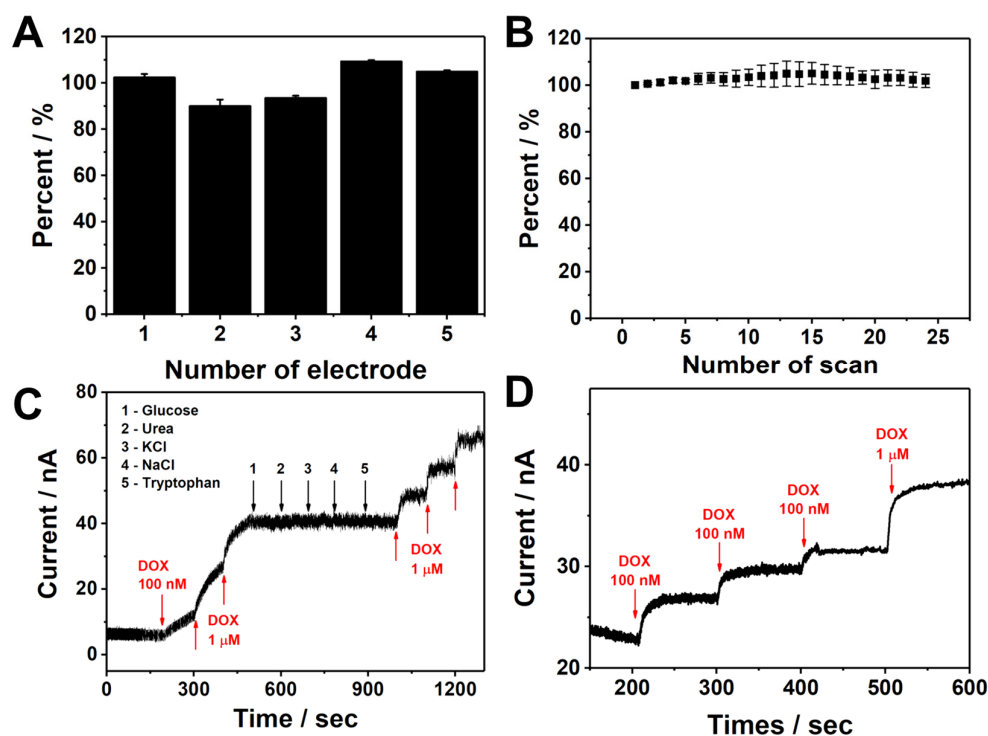


Figure 6. (A) The reproducibility for five different G/C@ErGO-GCE. (B) Stability over 24 scans for G/C@ErGO-GCE. (C) The amperometric response of G/C@ErGO-GCE to the successive addition of 100 nM and 1 μM DOX, 10 μM glucose, 10 μM urea, 10 μM KCl, 10 μM NaCl, 10 μM tryptophan. (D) Real-sample detection of DOX with 10 mM PBS buffer saline containing 10% human serum media by using G/C@ErGO-GCE.

Stability is important for evaluating the chemical and physical stability of the bio-nanohybrid composite electrode. The stability of G/C@ErGO-GCE was assessed by comparing the electrochemical signal over successive CV scans. Figure 6B represents the electrochemical signal changes with the number of cycles. The sensor showed no significant change in electrochemical signals even after twenty-four scans, with a low RSD value of 3.66%, indicating good stability.

Selectivity is an important factor for evaluating the performance of a sensor. The selectivity of G/C@ErGO-GCE was evaluated by comparing its amperometric response to DOX with its response to interfering substances, including glucose, urea, KCl, NaCl, and tryptophan. These interfering substances were chosen due to their presence in biological fluids and their chemical structure similarities. As shown in Figure 6C, there was no significant increase in current upon the addition of 10 μM of these interfering substances, while the current increased upon the addition of DOX. This result indicates that G/C@ErGO-GCE has optimal selectivity for detecting DOX, even in the presence of higher concentrations of interfering substances.

Real-sample detection is essential for evaluating the sensing performance within biological fluids for the practical application of the G/C@ErGO-GCE sensor. Human serum diluted with 10 mM PBS buffer saline was introduced for real-sample detection to mimic complex biological fluids. The amperometric response showed significant increases upon the addition of DOX, demonstrating the potential for the practical application of the G/C@ErGO-GCE sensor (Figure 6D).

4. Conclusions

We have demonstrated the facile fabrication of G/C@ErGO-GCE and evaluated its sensing performance for DOX. The bio-nano hybrid electrode of G/C@ErGO was successfully fabricated using a simple electrochemical reduction and drop-casting method. The fabricated G/C@ErGO-GCE was characterized by SEM, AFM, contact angle measurement, XPS, CV, EIS, and Raman spectroscopy. The results of the physical and chemical characterization of the G/C@ErGO bio-nano hybrid composite confirm that our fabrication process is suitable and reliable. The G/C@ErGO-GCE exhibited promising characteristics, including favorable electrochemical properties, surface wettability, and I_D/I_G values, leading to enhanced DOX detection. These improvements are attributed to the immobilized G/C single nucleotides functioning as receptor moieties. Additionally, the G/C@ErGO-GCE demonstrated superior analytical performance, including sensitivity, selectivity, stability, and reproducibility in DOX detection using DPV and CA. The sensing performance of G/C@ErGO-GCE was further confirmed within the biological fluid of human serum, indicating its potential for practical application. As the proposed sensing mechanism remains partially studied, we will conduct a comprehensive investigation in future work, using various experimental techniques and computational modeling, including molecular dynamics simulations. Therefore, the proposed electrochemical sensor could serve as a potent tool for drug development and pharmacokinetic studies.

Supplementary Materials: The following supporting information can be downloaded at: <https://www.mdpi.com/article/10.3390/chemosensors12080163/s1>, Scheme S1: Explanation for binding events between guanine/cytosine and doxorubicin; Figure S1: Electrochemical reduction of graphene oxide with cyclic voltammetry; Figure S2: AFM images of (A) bare GCE, (B) ErGO-GCE, and (C) G/C@ErGO-GCE. Height profiles for determining height differences on (D) bare GCE, (E) ErGO-GCE, and (F) G/C@ErGO-GCE. (G) Plot of the height differences obtained from (D–F). (H) Comparison of the average height differences and RSD value for each electrode; Figure S3: Optimization of guanine and cytosine ratio. Each plot represents the oxidation peak current of DOX at different concentrations from 10 nM to 1 μ M with different guanine and cytosine ratio of (A) 0:10, (B) 1:9, (C) 3:7, (D) 5:5, (E) 7:3, (F) 9:1, and (G) 10:0 (guanine:cytosine), respectively; Figure S4: DPV curves for the DOX detection with (A) bare GCE and (B) ErGO-GCE.

Author Contributions: Conceptualization, C.-S.L.; methodology, Y.C.; software, Y.C. and T.H.K.; validation, D.E.O. and M.K.; formal analysis, Y.C.; investigation, M.K. and A.L.; resources, T.H.K.; data curation, D.E.O.; writing—original draft preparation, C.-S.L. and D.E.O.; writing—review and editing, T.H.K.; visualization, M.K., A.L. and Y.C.; supervision, T.H.K.; project administration, T.H.K.; funding acquisition, C.-S.L. and T.H.K. All authors have read and agreed to the published version of the manuscript.

Funding: This research work was funded by Seoul Women’s University grant number 2023-0008 and the Soonchunhyang University Research Fund. In addition, this work was supported by a Korea Basic Science Institute (National Research Facilities and Equipment Center) grant funded by the Ministry of Education (2022R1A6C101B794).

Institutional Review Board Statement: Not applicable.

Informed Consent Statement: Not applicable.

Data Availability Statement: Data available on request from the authors.

Conflicts of Interest: The authors declare no conflicts of interest.

References

1. Akinwande, D.; Huyghebaert, C.; Wang, C.-H.; Serna, M.I.; Goossens, S.; Li, L.-J.; Wong, H.-S.P.; Koppens, F.H.L. Graphene and Two-Dimensional Materials for Silicon Technology. *Nature* **2019**, *573*, 507–518. [[CrossRef](#)] [[PubMed](#)]
2. Wu, Y.; Zhu, J.; Huang, L. A Review of Three-Dimensional Graphene-Based Materials: Synthesis and Applications to Energy Conversion/Storage and Environment. *Carbon* **2019**, *143*, 610–640. [[CrossRef](#)]
3. Han, S.; Sun, J.; He, S.; Tang, M.; Chai, R. The Application of Graphene-Based Biomaterials in Biomedicine. *Am. J. Transl. Res.* **2019**, *11*, 3246–3260. [[PubMed](#)]

4. Song, S.; Shen, H.; Wang, Y.; Chu, X.; Xie, J.; Zhou, N.; Shen, J. Biomedical Application of Graphene: From Drug Delivery, Tumor Therapy, to Theranostics. *Colloids Surf. B Biointerfaces* **2020**, *185*, 110596. [[CrossRef](#)] [[PubMed](#)]
5. Papageorgiou, D.G.; Kinloch, I.A.; Young, R.J. Mechanical Properties of Graphene and Graphene-Based Nanocomposites. *Prog. Mater. Sci.* **2017**, *90*, 75–127. [[CrossRef](#)]
6. Akinwande, D.; Brennan, C.J.; Bunch, J.S.; Egberts, P.; Felts, J.R.; Gao, H.; Huang, R.; Kim, J.-S.; Li, T.; Li, Y.; et al. A Review on Mechanics and Mechanical Properties of 2D Materials—Graphene and Beyond. *Extrem. Mech. Lett.* **2017**, *13*, 42–77. [[CrossRef](#)]
7. Guo, B.; Fang, L.; Zhang, B.; Gong, J.R. Graphene Doping: A Review. *Insci. J.* **2011**, *1*, 80–89. [[CrossRef](#)]
8. Yang, Z.; Yao, Z.; Li, G.; Fang, G.; Nie, H.; Liu, Z.; Zhou, X.; Chen, X.; Huang, S. Sulfur-Doped Graphene as an Efficient Metal-Free Cathode Catalyst for Oxygen Reduction. *ACS Nano* **2012**, *6*, 205–211. [[CrossRef](#)]
9. Geng, D.; Yang, S.; Zhang, Y.; Yang, J.; Liu, J.; Li, R.; Sham, T.-K.; Sun, X.; Ye, S.; Knights, S. Nitrogen Doping Effects on the Structure of Graphene. *Appl. Surf. Sci.* **2011**, *257*, 9193–9198. [[CrossRef](#)]
10. Dai, J.; Yuan, J. Adsorption of Molecular Oxygen on Doped Graphene: Atomic, Electronic, and Magnetic Properties. *Phys. Rev. B* **2010**, *81*, 165414. [[CrossRef](#)]
11. Jose, P.P.A.; Kala, M.S.; Kalarikkal, N.; Thomas, S. Reduced Graphene Oxide Produced by Chemical and Hydrothermal Methods. *Mater. Today Proc.* **2018**, *5*, 16306–16312. [[CrossRef](#)]
12. Long, D.; Li, W.; Ling, L.; Miyawaki, J.; Mochida, I.; Yoon, S.-H. Preparation of Nitrogen-Doped Graphene Sheets by a Combined Chemical and Hydrothermal Reduction of Graphene Oxide. *Langmuir* **2010**, *26*, 16096–16102. [[CrossRef](#)]
13. Lee, C.-S.; Yu, S.; Kim, T. One-Step Electrochemical Fabrication of Reduced Graphene Oxide/Gold Nanoparticles Nanocomposite-Modified Electrode for Simultaneous Detection of Dopamine, Ascorbic Acid, and Uric Acid. *Nanomaterials* **2017**, *8*, 17. [[CrossRef](#)] [[PubMed](#)]
14. Lee, C.-S.; Oh, D.E.; Kim, T.H. Label-Free Assay of Protein Kinase A Activity and Inhibition in Cancer Cell Using Electrochemically-Prepared AuNP/rGO Nanohybrid Electrode Modified with C-Kemptide. *Talanta* **2020**, *215*, 120899. [[CrossRef](#)] [[PubMed](#)]
15. Oh, D.E.; Lee, C.-S.; Kim, T.H. Simultaneous and Individual Determination of Seven Biochemical Species Using a Glassy Carbon Electrode Modified with a Nanocomposite of Pt Nanoparticle and Graphene by a One-Step Electrochemical Process. *Talanta* **2022**, *247*, 123590. [[CrossRef](#)] [[PubMed](#)]
16. Yuan, L.; Liu, L. Peptide-Based Electrochemical Biosensing. *Sens. Actuators B Chem.* **2021**, *344*, 130232. [[CrossRef](#)]
17. Vanova, V.; Mitrevska, K.; Milosavljevic, V.; Hynek, D.; Richtera, L.; Adam, V. Peptide-Based Electrochemical Biosensors Utilized for Protein Detection. *Biosens. Bioelectron.* **2021**, *180*, 113087. [[CrossRef](#)]
18. Jang, S.J.; Lee, C.-S.; Kim, T.H. α -Synuclein Oligomer Detection with Aptamer Switch on Reduced Graphene Oxide Electrode. *Nanomaterials* **2020**, *10*, 832. [[CrossRef](#)]
19. Lee, C.-S.; Yu, S.H.; Kim, T.H. A “Turn-on” Electrochemical Aptasensor for Ultrasensitive Detection of Cd²⁺ Using Duplexed Aptamer Switch on Electrochemically Reduced Graphene Oxide Electrode. *Microchem. J.* **2020**, *159*, 105372. [[CrossRef](#)]
20. Huizenga, D.E.; Szostak, J.W. A DNA Aptamer That Binds Adenosine and ATP. Available online: <https://pubs.acs.org/doi/pdf/10.1021/bi00002a033> (accessed on 20 June 2024).
21. Breaker, R.R. DNA Aptamers and DNA Enzymes. *Curr. Opin. Chem. Biol.* **1997**, *1*, 26–31. [[CrossRef](#)]
22. Sharma, T.K.; Bruno, J.G.; Dhiman, A. ABCs of DNA Aptamer and Related Assay Development. *Biotechnol. Adv.* **2017**, *35*, 275–301. [[CrossRef](#)] [[PubMed](#)]
23. Hynek, D.; Krejcová, L.; Zitka, O.; Adam, V.; Trnkova, L.; Sochor, J.; Stiborova, M.; Eckschlager, T.; Hubalek, J.; Kizek, R. Electrochemical Study of Doxorubicin Interaction with Different Sequences of Single Stranded Oligonucleotides, Part I. *Int. J. Electrochem. Sci.* **2012**, *7*, 13–33. [[CrossRef](#)]
24. Jawad, B.; Poudel, L.; Podgornik, R.; Ching, W.-Y. Thermodynamic Dissection of the Intercalation Binding Process of Doxorubicin to dsDNA with Implications of Ionic and Solvent Effects. *J. Phys. Chem. B* **2020**, *124*, 7803–7818. [[CrossRef](#)]
25. Gnapareddy, B.; Reddy Dugasani, S.; Ha, T.; Paulson, B.; Hwang, T.; Kim, T.; Hoon Kim, J.; Oh, K.; Park, S.H. Chemical and Physical Characteristics of Doxorubicin Hydrochloride Drug-Doped Salmon DNA Thin Films. *Sci. Rep.* **2015**, *5*, 12722. [[CrossRef](#)]
26. Shandilya, M.; Sharma, S.; Das, P.P.; Charak, S.; Shandilya, M.; Sharma, S.; Das, P.P.; Charak, S. Molecular-Level Understanding of the Anticancer Action Mechanism of Anthracyclines. In *Advances in Precision Medicine Oncology*; IntechOpen: London, UK, 2020; ISBN 978-1-83968-868-3.
27. Vail, D.M.; Amantea, M.A.; Colbern, G.T.; Martin, F.J.; Hilger, R.A.; Working, P.K. Pegylated Liposomal Doxorubicin: Proof of Principle Using Preclinical Animal Models and Pharmacokinetic Studies. *Semin. Oncol.* **2004**, *31*, 16–35. [[CrossRef](#)] [[PubMed](#)]
28. Trevisan, M.G.; Poppi, R.J. Determination of Doxorubicin in Human Plasma by Excitation–Emission Matrix Fluorescence and Multi-Way Analysis. *Anal. Chim. Acta* **2003**, *493*, 69–81. [[CrossRef](#)]
29. Sakai-Kato, K.; Saito, E.; Ishikura, K.; Kawanishi, T. Analysis of Intracellular Doxorubicin and Its Metabolites by Ultra-High-Performance Liquid Chromatography. *J. Chromatogr. B* **2010**, *878*, 1466–1470. [[CrossRef](#)]
30. Arnold, R.D.; Slack, J.E.; Straubinger, R.M. Quantification of Doxorubicin and Metabolites in Rat Plasma and Small Volume Tissue Samples by Liquid Chromatography/Electrospray Tandem Mass Spectroscopy. *J. Chromatogr. B* **2004**, *808*, 141–152. [[CrossRef](#)]
31. Lee, C.-S.; Shim, S.J.; Kim, T.H. Scalable Preparation of Low-Defect Graphene by Urea-Assisted Liquid-Phase Shear Exfoliation of Graphite and Its Application in Doxorubicin Analysis. *Nanomaterials* **2020**, *10*, 267. [[CrossRef](#)]
32. Frederick, C.A.; Williams, L.D.; Ughetto, G.; Van der Marel, G.A.; Van Boom, J.H.; Rich, A.; Wang, A.H.J. Structural comparison of anticancer drug-DNA complexes: Adriamycin and daunomycin. *Biochemistry* **1990**, *29*, 2538–2549. [[CrossRef](#)]

33. Trnkova, L.; Huska, D.; Adam, V.; Kizek, R.; Eckschlager, T.; Stiborova, M.; Hubalek, J. Electrochemical biosensor for investigation of anticancer drugs interactions (doxorubicin and ellipticine) with DNA. *IEEE Sens.* 2009. [[CrossRef](#)]
34. Hajiana, R.; Tayebib, Z.; Shams, N. Fabrication of an electrochemical sensor for determination of doxorubicin in human plasma and its interaction with DNA. *J. Pharm. Anal.* **2017**, *7*, 27–33. [[CrossRef](#)]
35. Zaaba, N.I.; Foo, K.L.; Hashim, U.; Tan, S.J.; Liu, W.-W.; Voon, C.H. Synthesis of Graphene Oxide Using Modified Hummers Method: Solvent Influence. *Procedia Eng.* **2017**, *184*, 469–477. [[CrossRef](#)]
36. Shahriary, L.; Athawale, A.A. Graphene Oxide Synthesized by Using Modified Hummers Approach. *Int. J. Energy Environ. Eng.* **2014**, *2*, 58–63.
37. Breazu, C.; Socol, M.; Preda, N.; Rasoga, O.; Costas, A.; Socol, G.; Petre, G.; Stanculescu, A. Nucleobases Thin Films Deposited on Nanostructured Transparent Conductive Electrodes for Optoelectronic Applications. *Sci. Rep.* **2021**, *11*, 7551. [[CrossRef](#)]
38. Melucci, M.; Treossi, E.; Ortolani, L.; Giambastiani, G.; Morandi, V.; Klar, P.; Casiraghi, C.; Samori, P.; Palermo, V. Facile Covalent Functionalization of Graphene Oxide Using Microwaves: Bottom-up Development of Functional Graphitic Materials. *J. Mater. Chem.* **2010**, *20*, 9052–9060. [[CrossRef](#)]
39. He, D.; Peng, Z.; Gong, W.; Luo, Y.; Zhao, P.; Kong, L. Mechanism of a Green Graphene Oxide Reduction with Reusable Potassium Carbonate. *RSC Adv.* **2015**, *5*, 11966–11972. [[CrossRef](#)]
40. Claramunt, S.; Varea, A.; López-Díaz, D.; Velázquez, M.M.; Cornet, A.; Cirera, A. The Importance of Interbands on the Interpretation of the Raman Spectrum of Graphene Oxide. *J. Phys. Chem. C* **2015**, *119*, 10123–10129. [[CrossRef](#)]
41. Abhishek Singh, T.; Sharma, V.; Thakur, N.; Tejwan, N.; Sharma, A.; Das, J. Selective and Sensitive Electrochemical Detection of Doxorubicin via a Novel Magnesium Oxide/Carbon Dot Nanocomposite Based Sensor. *Inorg. Chem. Commun.* **2023**, *150*, 110527. [[CrossRef](#)]
42. Ehsani, M.; Soleymani, J.; Mohammadalizadeh, P.; Hasanzadeh, M.; Jouyban, A.; Khoubnasabjafari, M.; Vaez-Gharamaleki, Y. Low Potential Detection of Doxorubicin Using a Sensitive Electrochemical Sensor Based on Glassy Carbon Electrode Modified with Silver Nanoparticles-Supported Poly(Chitosan): A New Platform in Pharmaceutical Analysis. *Microchem. J.* **2021**, *165*, 106101. [[CrossRef](#)]
43. Rong, S.; Zou, L.; Meng, L.; Yang, X.; Dai, J.; Wu, M.; Qiu, R.; Tian, Y.; Feng, X.; Ren, X.; et al. Dual Function Metal-Organic Frameworks Based Ratiometric Electrochemical Sensor for Detection of Doxorubicin. *Anal. Chim. Acta* **2022**, *1196*, 339545. [[CrossRef](#)] [[PubMed](#)]
44. Kong, F.; Luo, J.; Jing, L.; Wang, Y.; Shen, H.; Yu, R.; Sun, S.; Xing, Y.; Ming, T.; Liu, M.; et al. Reduced Graphene Oxide and Gold Nanoparticles-Modified Electrochemical Aptasensor for Highly Sensitive Detection of Doxorubicin. *Nanomaterials* **2023**, *13*, 1223. [[CrossRef](#)] [[PubMed](#)]
45. Skalová, Š.; Langmaier, J.; Barek, J.; Vyskočil, V.; Navrátil, T. Doxorubicin Determination Using Two Novel Voltammetric Approaches: A Comparative Study. *Electrochim. Acta* **2020**, *330*, 135180. [[CrossRef](#)]

Disclaimer/Publisher’s Note: The statements, opinions and data contained in all publications are solely those of the individual author(s) and contributor(s) and not of MDPI and/or the editor(s). MDPI and/or the editor(s) disclaim responsibility for any injury to people or property resulting from any ideas, methods, instructions or products referred to in the content.